

*Communications in
Applied
Mathematics and
Computational
Science*

A VOLUME-OF-FLUID
INTERFACE RECONSTRUCTION ALGORITHM
THAT IS
SECOND-ORDER ACCURATE IN THE MAX NORM

ELBRIDGE GERRY PUCKETT

vol. 5 no. 2 2010

A VOLUME-OF-FLUID INTERFACE RECONSTRUCTION ALGORITHM THAT IS SECOND-ORDER ACCURATE IN THE MAX NORM

ELBRIDGE GERRY PUCKETT

In an article recently published in this journal the author proved there exists a two-dimensional, volume-of-fluid interface reconstruction method that is second-order accurate in the max norm. However, that article did not include an example of such an algorithm. This article contains a description of a two-dimensional, volume-of-fluid interface reconstruction method that is second-order accurate in the max norm, provided the curve that one is reconstructing is two times continuously differentiable and the length of the sides of the square grid cells is less than a constant divided by the maximum of the absolute value of the curvature of the interface. A computation made with this algorithm is presented that demonstrates the convergence rate is second-order, as expected.

1. Introduction

Let $\Omega \in R^2$ denote a two-dimensional computational domain and take an oriented curve in Ω parametrized by $z(s) = (x(s), y(s))$, where $0 \leq s \leq s_{\text{end}}$ is arc length. Let L be a characteristic length of the computational domain Ω . Cover Ω with a grid consisting of square cells each of side $\Delta x \leq L$ and let

$$h = \frac{\Delta x}{L} \tag{1}$$

be a dimensionless parameter that represents the size of a grid cell. Note that h is bounded above by 1. For the remainder of this article it is to be understood that quantities such as the arc length s are also nondimensional quantities that have been obtained by division by L as in (1), and that the curvature κ has been nondimensionalized by dividing by $1/L$.

MSC2000: primary 76-04, 65M06, 65M15, 76M20, 76M25; secondary 74A50, 94A08, 74S99, 76T99.

Keywords: volume-of-fluid, interface reconstruction, front reconstruction, piecewise linear interface reconstruction, fronts, two-phase flow, multiphase systems, adaptive mesh refinement, computational fluid dynamics.

Sponsored by the U.S. Department of Energy Mathematical, Information, and Computing Sciences Division contracts DE-FC02-01ER25473 and DE-FG02-03ER25579.

The *volume-of-fluid interface reconstruction problem* is to compute an approximation $\tilde{z}(s)$ to $z(s)$ in Ω using only the volume fractions Λ_{ij} associated with the curve z on the grid. In this paper the convention will be that the volume fraction Λ_{ij} in the ij -th cell is the fraction of material that lies in the ij -th cell on the “outside” of $z(s)$ — that is, on the side towards which the outward pointing unit normal vector n to the interface $z(s)$ points.

The purpose of this article is to describe a new volume-of-fluid method for reconstructing the interface $z(s) = (x(s), y(s))$ between two materials that is second-order accurate in the max norm. The main result in [24; 25] is a proof that

$$|g(x) - \tilde{g}_{ij}(x)| \leq \left(\frac{50}{3}\kappa_{\max} + C_S\right)h^2 \quad \text{for all } x \in [x_i, x_{i+1}], \quad (2)$$

where $(x, \tilde{g}_{ij}(x))$ is the volume-of-fluid approximation to the interface¹ $(x, g(x))$ described in this paper; κ_{\max} is the maximum of the absolute value of the curvature of the interface in the 3×3 block of cells B_{ij} centered on the cell C_{ij} in which one wishes to reconstruct the interface; $x = x_i$ and $x = x_{i+1}$ are the x -coordinates of the left and right edges of the cell $C_{ij} = [x_i, x_{i+1}] \times [y_j, y_{j+1}]$ in which one wishes to reconstruct the interface; $h = \Delta x/L$ is the length defined in (1) of the edges of the square grid cells; and

$$C_S = \frac{\sqrt{3}}{2} \left\{ (2\sqrt{2} - 1)4\sqrt{\kappa_{\max}} + \left(1 - \frac{7(1+\sqrt{2})}{20}\right) \frac{32}{3} (\sqrt{\kappa_{\max}})^3 \right\}^2. \quad (3)$$

The bound in (2) holds whenever the grid size h and the maximum κ_{\max} of the absolute value of the curvature $\kappa(s)$ of the interface $z(s)$

$$\kappa_{\max} = \max_s |\kappa(s)| \quad (4)$$

satisfies²

$$h \leq \frac{C_h}{\kappa_{\max}}, \quad (5)$$

where

$$C_h = \frac{1}{25}. \quad (6)$$

¹As explained in the following paragraph, it is proven in [24] that the constraint on h in terms of κ_{\max} in (5) ensures that one can reparametrize the interface as $y = g(x)$ or $x = G(y)$ locally about the cell $C_{ij} = [x_i, x_{i+1}] \times [y_j, y_{j+1}]$ in which one wishes to reconstruct the interface. For convenience, in this article the interface will frequently be written as $y = g(x)$ instead of $z(s)$, it being understood that in some cells the parametrizations has to be $x = G(y)$.

²It is only necessary that this condition be satisfied in a neighborhood of the cell C_{ij} ; for example, in the 3×3 block of cells B_{ij} centered on the cell C_{ij} .

Section 2 of [24] contains a proof that the constraint in (5) on h is sufficient to ensure that the interface $z(s) = (x(s), y(s))$ can be written as a single valued function $y = g(x)$ or $x = G(y)$ on any 3×3 block of cells B_{ij} centered on a cell C_{ij} which contains a portion of the interface.³

In the algorithm described in this article one uses the row of three cells above and below B_{ij} to determine which columns to use in the approximation to the slope m_{ij} of the piecewise linear approximation

$$\tilde{g}_{ij}(x) = m_{ij}x + b_{ij} \tag{7}$$

to the interface $y = g(x)$. For this reason one must consider the 5×5 block of cells \tilde{B}_{ij} centered on the cell C_{ij} . However, as shown in Section 5, once one has rotated the block \tilde{B}_{ij} so that the interface only enters (resp., exits) the 3×3 subblock B_{ij} across its left or top edge (resp., top or right edge); it is not necessary to use the first and last columns of the larger block of cells \tilde{B}_{ij} .

The articles [24; 25] consist solely of a collection of proofs showing that *there exists* a volume-of-fluid interface reconstruction algorithm that is second-order accurate in the max norm; that is, *they do not contain an example of such an algorithm*. However, the proofs in [24; 25] are constructive, and the algorithm described here is based on those proofs. To date, no other volume-of-fluid interface reconstruction algorithms have been proven to be second-order accurate in the max norm. Section 6 contains a computational example to demonstrate that this algorithm produces an approximation to $\cos x$ for $0 \leq x \leq \pi$ that is a second-order accurate in the max norm.

A detailed statement of the problem. Suppose that one is given a simply connected computational domain $\Omega \in R^2$ that is divided into two distinct, disjoint regions Ω_1 and Ω_2 such that $\Omega_1 \cup \Omega_2 = \Omega$. Let Ω_1 be referred to as material 1 and Ω_2 as material 2. (Although these algorithms have historically been known as “volume-of-fluid” methods, they are frequently used to model the interface between any two materials, including gases, liquids, solids and any combination thereof; for example, see [5; 14; 15; 16].)

Let $z(s) = (x(s), y(s))$, where s is arc length, denote the *interface* between these two materials and assume that the interface has been oriented so that as one traverses the interface with increasing arc length material 1 lies to the right. Cover Ω with a uniform square grid of cells, each with side h , and let Λ_{ij} denote the fraction of material 1 in the ij -th cell.

³In that article and this one interfaces that are undergoing topological changes, such as when a droplet separates into two droplets, are not considered. In order for this algorithm to achieve second-order accuracy, the interface must be a *single-valued* C^2 function in the 3×3 block B_{ij} surrounding the cell C_{ij} .

Each number Λ_{ij} satisfies $0 \leq \Lambda_{ij} \leq 1$ and is called the *volume fraction* (of material 1) in the ij -th cell.⁴ Note that

$$0 < \Lambda_{ij} < 1 \quad (8)$$

if and only if a portion of the interface $z(s)$ lies in the ij -th cell. Similarly, $\Lambda_{ij} = 1$ means the ij -th cell only contains material 1, and $\Lambda_{ij} = 0$ means it only contains material 2.

Consider the following problem. Given only the collection of volume fractions Λ_{ij} in the grid covering Ω , *reconstruct* $z(s)$; in other words, find a piecewise linear approximation \tilde{z} to z in each cell C_{ij} that contains a portion of the interface $z(s)$. Furthermore, the approximate interface \tilde{z} must have the property that the volume fractions $\tilde{\Lambda}_{ij}$ due to \tilde{z} are identical to the original volume fractions Λ_{ij} ; that is,

$$\tilde{\Lambda}_{ij} = \Lambda_{ij} \quad \text{for all cells } C_{ij}. \quad (9)$$

An algorithm for finding such an approximation is known as a *volume-of-fluid interface reconstruction method*.

The property that $\tilde{\Lambda}_{ij} = \Lambda_{ij}$ is the principal feature that distinguishes volume-of-fluid interface reconstruction methods from other interface reconstruction methods. This ensures that the computational value of the total volume of each material is conserved. In other words, all volume-of-fluid interface reconstruction methods are conservative in that they conserve the volume of each material in the computation. When the underlying numerical method is a conservative finite difference method that one is using to model a system of hyperbolic conservation laws (e.g., gas dynamics) this can be essential since, for example, in order to obtain the correct shock speed it is necessary for all of the conserved quantities to be conserved by the underlying numerical method [13]. More generally, a necessary condition for the numerical method to converge to the correct weak solution of a system of hyperbolic conservation laws is that all of the quantities that are conserved in the underlying partial differential equation must be conserved by the numerical method [12].

Volume-of-fluid methods have been used by researchers to track material interfaces since at least the mid 1970s [18; 19]. Researchers have developed a variety of volume-of-fluid algorithms for modeling everything from flame propagation [3] to curvature and solidification [4]. In particular, the problem of developing high-order accurate volume-of-fluid methods for modeling the curvature and surface tension of an interface has received a lot of attention [1; 2; 4; 7; 32; 22]. Volume-of-fluid methods were among the first interface tracking algorithms to be implemented in codes originally developed at the U.S. National Laboratories, and subsequently

⁴Even though in two dimensions Λ_{ij} is technically an area fraction, the convention is to refer to it as a *volume fraction*.

released to the general public, that were capable of tracking material interfaces in a variety of complex material flow problems [6; 9; 17; 30; 31]. They continue to be widely used at these institutions, as well as by the general scientific community.

This article does not contain work concerning the related problem of approximating the movement of the interface in time, for which one would use a *volume-of-fluid advection algorithm*. The interested reader may wish to consult [21; 27; 28] for a detailed description and analysis of several such algorithms. In this article only the accuracy that one can obtain when using a volume-of-fluid interface reconstruction algorithm to approximate a given *stationary* interface $z(s)$ is considered.

2. Assumptions and definitions

Notation. The *center cell* $C_{ij} = [x_i, x_{i+1}] \times [y_j, y_{j+1}]$ is the square grid cell with side h that contains a portion of the interface $z(s) = (x(s), y(s))$ for s in some interval, say $s \in (s_l, s_r)$, in which one wishes to reconstruct the interface. This is equivalent to saying that $0 < \Lambda_{ij} < 1$. In what follows the 5×5 block of square cells — each with side h — centered on the center cell C_{ij} , as shown, for example, in Figure 1, will be denoted $\tilde{B}_{ij} = [x_{i-2}, x_{i+3}] \times [y_{j-2}, y_{j+3}]$. In addition, the subblock of \tilde{B}_{ij} which consists of the 3×3 subblock of cells centered on the cell

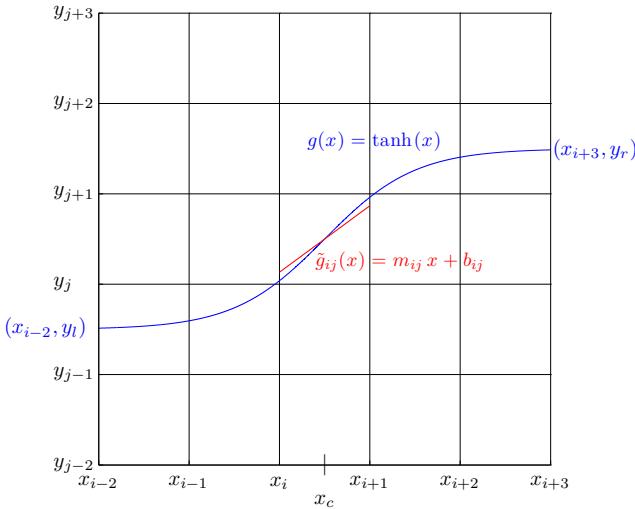


Figure 1. In this example the interface is $g(x) = \tanh(x)$ and material 1 lies *below* the curve. Note that all three of the column sums are *exact*, but that for the inverse function $x = g^{-1}(y)$, only the (horizontal) center column sum is exact. (Exact column sums are defined in Section 4 below.) The cell in which one wishes to reconstruct the interface is C_{ij} , the 3×3 block of cells centered on C_{ij} is B_{ij} , and the 5×5 block of cells centered on C_{ij} is \tilde{B}_{ij} .

C_{ij} will be denoted $B_{ij} = [x_{i-1}, x_{i+2}] \times [y_{j-1}, y_{j+2}]$, and the 3×5 subblock of \tilde{B}_{ij} , which is B_{ij} together with the row of 3 cells $C_{i-1,j-2}$, C_{ij-2} and $C_{i+1,j-2}$ added to its bottom and the row of 3 cells $C_{i-1,j+2}$, $C_{i,j+2}$ and $C_{i+1,j+2}$ added to its top, will be denoted $\hat{B}_{ij} = [x_{i-1}, x_{i+2}] \times [y_{j-2}, y_{j+3}]$. The coordinates of the vertical edges of the cells in \tilde{B}_{ij} are denoted $x_{i-2}, x_{i-1}, x_i, x_{i+1}, x_{i+2}$ and x_{i+3} and the horizontal edges by $y_{j-2}, y_{j-1}, y_j, y_{j+1}, y_{j+2}$ and y_{j+3} as shown, for example, in Figure 1.⁵ It will always be the case that $x_{i+1} - x_i = h, y_{j+1} - y_j = h$, etc.

Assumptions concerning the interface. In this article the exact interface

$$z(s) = ((x(s), y(s)))$$

is assumed to satisfy the following conditions:

- I. The interface z is two times continuously differentiable; in other words,

$$z(s) \in C^2(\Omega). \tag{10}$$

- II. The grid size h and the maximum value

$$\kappa_{\max} = \max_s |\kappa(s)|$$

of the absolute value of the curvature $\kappa(s)$ of the interface satisfy the following constraint in terms of each other:⁶

$$h \leq \frac{C_h}{\kappa_{\max}}, \tag{11}$$

where

$$C_h = \frac{1}{25}.$$

Remark. One can show that the constraint in (11) prevents configurations in which the interface enters the center cell C_{ij} , exits it, and then enters it again, before exiting the 5×5 block of cells \tilde{B}_{ij} , as shown in Figure 2. In particular, one can use the constraint in (11) to show that the interface does not have hairpin turns which are on the order of a grid cell. See [24] for a proof of these facts.

Note that it may be possible for the interface to pass through the center cell, then exit the 3×3 block B_{ij} , “wander around the computational domain”, and then reenter the 3×3 block B_{ij} and the center cell C_{ij} again. The constraint in (11) simply guarantees that given a point on the interface that lies in the center cell C_{ij} , one can find an orientation of the 3×3 block B_{ij} such that *locally* the interface can be written as a single-valued function on the interval $[x_{i-1}, x_{i+2}]$ such that the

⁵Whenever possible, the same notation is used in this article as in [24; 25]. One significant change, however, is that the lower left corner of the center cell C_{ij} is now (x_i, y_j) rather than (x_{i-1}, y_{j-1}) as it was denoted in [24].

⁶See footnote 2.

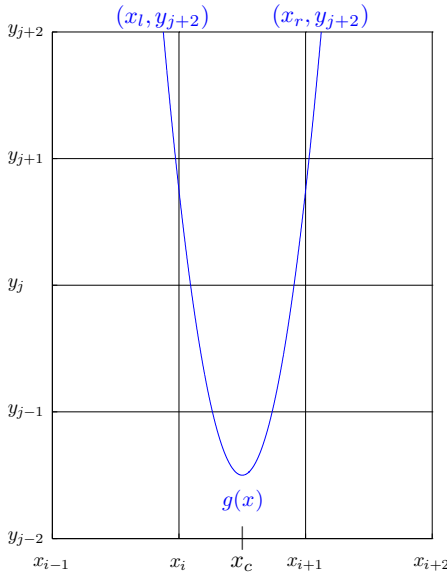


Figure 2. In this example, $h = 1$ and the interface is the parabola $g(x) = a(x - x_c)^2 - \frac{1}{2}$ with $a = 9$. Consequently, the maximum curvature of the interface is

$$\kappa_{\max} = 2a = 18 > C_h h^{-1} = \frac{1}{25},$$

and hence the constraint on the cell size h in (5) is not satisfied. As one can see from the figure, the interface enters the 3×3 block of cells B_{ij} through the top edge of the left column, passes through the center cell C_{ij} , exits the 3×3 block of cells B_{ij} through the bottom edge of the center column (i.e., the line $y = y_{j-1}$), and then passes through B_{ij} again; the second path being a reflection about the line $x = x_c$ of the first. The constraint on h with respect to the maximum curvature κ_{\max} in (5) ensures that the interface does not have sharp or “hairpin” turns that are on the scale of the 3×3 block of cells B_{ij} , such as the one illustrated here. A finer grid (i.e., smaller h) is required in order to resolve curves such as this one.

curve enters the 3×3 block B_{ij} , passes through the center cell once — and only once — and then exits B_{ij} . It does not prevent the curve from eventually reentering the center cell after traversing the domain for a large number of cell lengths. In this article it is assumed that this latter case does not occur.

3. Rotation of the 5 by 5 block

Given a cell C_{ij} that contains a portion $y = g(x)$ of the interface, or equivalently, a cell C_{ij} in which $0 < \Lambda_{ij} < 1$, assume that the 5×5 block of cells \tilde{B}_{ij} centered on C_{ij} has been rotated so that *in the rotated coordinate frame* the bottom row of cells in the 3×5 subblock of cells \hat{B}_{ij} satisfy

$$\Lambda_{i-1,j-2} = 1, \quad \Lambda_{ij-2} = 1, \quad \Lambda_{i+1,j-2} = 1.$$

This ensures that the interface does not exit the 3×5 subblock of cells \hat{B}_{ij} across its bottom edge. Not only does this reduce the number of cases that one must consider in the description of the algorithm, but it also reduces the number of cases one must consider in the implementation of the algorithm. This is because the *Symmetry Lemma* of [24, page 119] states that all configurations of the interface with respect to the 3×3 block B_{ij} are equivalent to the following two cases:

Configuration A: The interface enters B_{ij} across the left edge of B_{ij} and exits across the right edge of B_{ij} (as shown, for example, in Figure 1).

Configuration B: The interface enters B_{ij} across the left edge of B_{ij} and exits across the top edge of B_{ij} (as shown, for example, in Figure 4).

Provided only that the interface satisfies the conditions in (5) and (10), these two cases are equivalent to all of the other ways in which the interface can enter the 3×3 block of cells B_{ij} , pass through the center cell C_{ij} , and exit the block B_{ij} . In other words, rotating the block B_{ij} by 0, 90, 180 or 270 degrees and/or interchanging the direction traversed by the arc length parameter $s \rightarrow -s$, one can arrive at a configuration that is identical to one of the two configurations listed above. This is a consequence of the Symmetry Lemma cited above.

In the implementation of this algorithm, for the purposes of producing the results shown in Section 6, the case in which—after the 5×5 block of cells \tilde{B}_{ij} has been rotated—the interface enters B_{ij} across the top edge and exits it across the right edge is also included. In other words, the symmetric image of the example shown in Figure 4 is also included in this implementation of the algorithm, although according to the Symmetry Lemma this is not strictly necessary.

During the course of proving the results in [24; 25], or in developing a second-order accurate volume-of-fluid interface reconstruction method such as the one described here, it is often necessary to rotate the 5×5 block of cells \tilde{B}_{ij} centered on C_{ij} by 90, 180, or 270 degrees and/or reflect the coordinates about one of the coordinate axes: $x \rightarrow -x$ or $y \rightarrow -y$. No other coordinate transformations besides one of these three rotations and a possible reversal of one or both of the variables $x \rightarrow -x$ and/or $y \rightarrow -y$ are required in order for the algorithm studied in this article and the articles in [24; 25] to converge to the exact interface as $h \rightarrow 0$. Furthermore,

these coordinate transformations are only used to determine a first-order accurate approximation m_{ij} to $g'(x_c)$ in the center cell. The grid covering the domain Ω always remains the same.

Thus, if one is using the interface reconstruction algorithm as part of a numerical method to solve a more complex problem than the one posed here (e.g., the movement of a fluid interface where the underlying fluid flow is a solution of the Euler or Navier–Stokes equations), it is not necessary to perform these coordinate transformations on the underlying numerical fluid flow solver. Therefore, unless noted otherwise, in what follows the interface will always be written $y = g(x)$ and the coordinates of the edges of the cells in the 3×3 block B_{ij} will be denoted by x_{i-1} , x_i , x_{i+1} , x_{i+2} and y_{j-1} , y_j , y_{j+1} , y_{j+2} , it being implicitly understood that a transformation of the coordinate system as described above may have been performed in order for this representation of the interface to be valid, and that the names of the variables x and y might have been interchanged in order to write the interface as $y = g(x)$.

4. Column sums

Let S_{i-1} , S_i and S_{i+1} represent the left, center and right *column sums* respectively in the 3×3 subblock of cells B_{ij} centered on C_{ij} :

$$S_{i-1} = \sum_{j'=j-1}^{j+1} \Lambda_{i-1,j'}, \quad S_i = \sum_{j'=j-1}^{j+1} \Lambda_{ij'}, \quad S_{i+1} = \sum_{j'=j-1}^{j+1} \Lambda_{i+1,j'}. \quad (12)$$

The volume fraction Λ_{ij} in the ij -th cell C_{ij} is a nondimensional way of storing the volume of material 1 in that cell, while the i -th *column sum* S_i defined above is a nondimensional way of storing the total volume of material 1 in the column of three cells centered on the ij -th cell, and similarly for S_{i-1} and S_{i+1} .

Now consider an arbitrary column consisting of three cells with left edge $x = x_i$ and right edge $x = x_{i+1}$. Furthermore, assume that the interface can be written as a function $y = g(x)$ on the interval $[x_i, x_{i+1}]$. Assume also that the interface enters the column through its left edge, exits the column through its right edge and does not cross the top or bottom edges of the column, as is the case with each of the columns S_{i-1} , S_i and S_{i+1} in the 3×3 subblock of cells B_{ij} centered on the cell of interest C_{ij} shown in the example in [Figure 1](#). Then, in particular, the total volume of material 1 that occupies the three cells of the center column and lies below the interface $g(x)$ is equal to the integral of $(g(x) - y_{j-1})$ over the interval $[x_i, x_{i+1}]$. This leads to the following relationship between the column sum and the normalized volume of material 1 in the column:

$$S_i = \sum_{j'=j-1}^{j+1} \Lambda_{ij'} = \frac{1}{h^2} \int_{x_i}^{x_{i+1}} (g(x) - y_{j-1}) dx. \quad (13)$$

This in turn leads to the following definition.

Definition. Assume that the interface $y = g(x)$ enters the i -th column through its left edge and exits the i -th column through its right edge and does not cross the top or bottom edges of the column. Then the column sum S_i is *exact* whenever (13) holds. Integrals such as the one on the right in (13) will be referred to as *the normalized integral of g in the i -th column.*⁷

Given the 3×3 block of cells B_{ij} surrounding a cell C_{ij} that contains a portion $y = g(x)$ of the interface, the accuracy of the algorithm described in this paper is based on how well the column sums S_{i-1} , S_i and S_{i+1} approximate the normalized integral of g in the $(i - 1)$ -st, i -th, and $(i + 1)$ -st column. This is because if two of the column sums $S_{i+\alpha}$ and $S_{i+\beta}$ with $\alpha, \beta = 1, 0, -1$ and $\alpha \neq \beta$ are exact, then the slope

$$m_{ij} = \frac{S_{i+\beta} - S_{i+\alpha}}{\beta - \alpha} \tag{14}$$

will be a first-order accurate approximation to $g'(x_c)$, where $x_c = \frac{1}{2}(x_{i+1} - x_i)$, as shown in (18) below. (This is Theorem 23 in [24].) It then follows that the piecewise linear approximation

$$\tilde{g}_{ij}(x) = m_{ij} x + b_{ij} \tag{15}$$

to the portion of the interface $g(x)$ in C_{ij} is pointwise second-order accurate, as shown in (19) below. (This is Theorem 24 in [24].) Therefore, one should use one of the following three slopes for m_{ij} in (15):

$$m_{ij}^l = (S_i - S_{i-1}), \quad m_{ij}^c = \frac{1}{2}(S_{i+1} - S_{i-1}), \quad m_{ij}^r = (S_{i+1} - S_i). \tag{16}$$

Example 1. In order to see why one of the three slopes in (16) will be the best choice for m_{ij} , consider the case when the interface is a line $g(x) = m x + b$. In this case the 3×3 subblock of cells B_{ij} has two exact column sums as shown in Figure 3. Note that in this particular orientation of B_{ij} , g has two exact column sums; namely the sums in the first and second columns. It is easy to check that

$$\begin{aligned} m &= \frac{1}{h^2} \int_{x_{i-1}}^{x_i} (g(x) - y_{j-1}) dx - \frac{1}{h^2} \int_{x_{i-2}}^{x_{i-1}} (g(x) - y_{j-1}) dx \\ &= (S_i - S_{i-1}) = m_{ij}^l. \end{aligned}$$

⁷In [24] an *exact column sum* was mistakenly defined as

$$S_i \equiv \sum_{j'=j-1}^{j+1} \Lambda_{ij'} = \frac{1}{h^2} \int_{x_i}^{x_{i+1}} (g(x) - y_{j-1}h) dx;$$

that is, $y_{j-1}h$ appears in the integrand, rather than just y_{j-1} . The correct definition appears here.

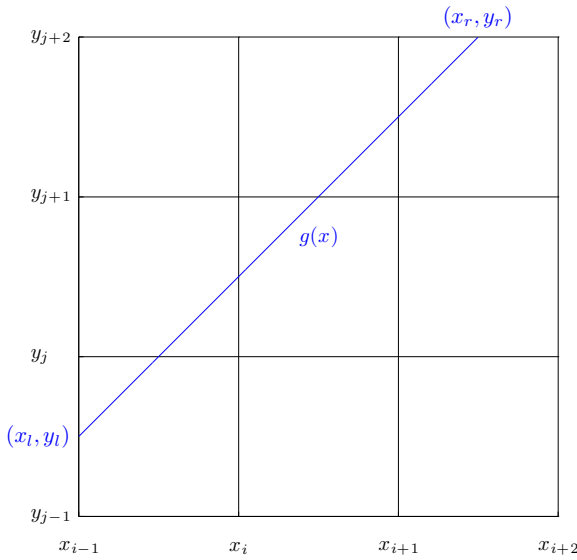


Figure 3. Here the interface g is a line $g(x) = m x + b$ that has two exact column sums; namely the sums in the first and second columns. In this case the slope m_{ij}^l from (16) is *exactly* equal to the slope m of the interface: $m_{ij}^l = m$. It is always the case that when the exact interface is a line on a grid of square cells one can find an orientation of the 3×3 block of cells B_{ij} such that at least one of the divided differences of the column sums in (16) is exact.

In this example the divided difference m_{ij}^l of the column sums S_{i-1} and S_i is *exactly* equal to the slope m of the exact interface. In fact, it is *always* the case that when the exact interface is a line and the grid consists of square cells, one can find an orientation of the 3×3 subblock of cells B_{ij} such that at least one of the divided differences of the column sums in (16) is exact. For example, note that in the case shown in Figure 3 one could rotate the 3×3 block of cells 90 degrees clockwise and then the correct slope to use when forming the piecewise linear approximation $\tilde{g}_{ij}(x) = m_{ij} x + b_{ij}$ would be $m_{ij} = m_{ij}^r$ in the rotated coordinate frame. One can easily check that this choice for m_{ij} would again be exactly equal to the slope m of the exact interface (in the rotated coordinate frame).

Example 2. However, as demonstrated in Example 2 of [25], there are instances in which the interface satisfies (5) but the center column sum S_i is not exact. An example was shown in Figure 4. All of the work in [25] is devoted to showing that when the interface satisfies (5), the center column sum S_i will still be exact to

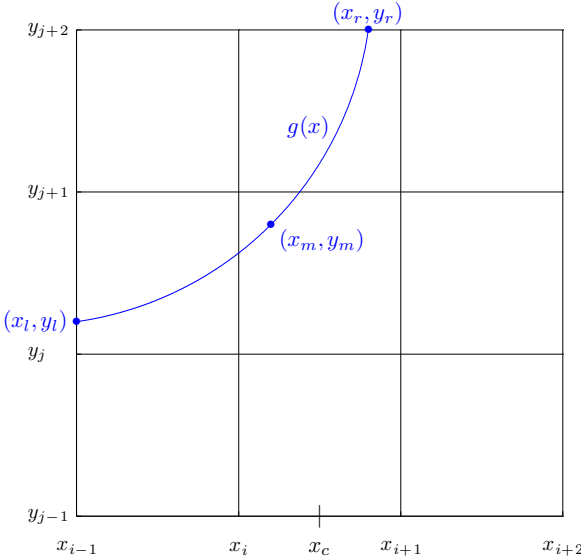


Figure 4. An example of a circular interface $g(x)$ that satisfies (5), but for which the center column sum is not exact in any of the four standard orientations of the grid. Consequently, any approximation m_{ij} to the slope $g'(x_c)$ of the form (14) must have a center column sum S_i that is not exact. (See [25, Example 2] for more details.) Theorem 4 of [25] states that if (5) is satisfied, then the error between the column sum S_i and the normalized integral of g over the center column is $O(h)$; that is, (5) implies that (17) holds. This suffices to ensure that (18) is true, and hence that (19) is true.

$O(h)$:⁸

$$\left| S_i - \frac{1}{h^2} \int_{x_i}^{x_{i+1}} (g(x) - y_{j-1}) dx \right| \leq C_S h, \tag{17}$$

where C_S is defined in (3). This is sufficient for either the left- or the right-sided difference in (16) to satisfy

$$|m_{ij} - g'(x_c)| \leq \left(\frac{26}{3} \kappa_{\max} + C_S \right) h, \tag{18}$$

where κ_{\max} is defined in (4). This, in turn, is sufficient for the piecewise linear volume-of-fluid approximation $\tilde{g}_{ij} = m_{ij} x + b_{ij}$ to still be second-order accurate

⁸In [24] the definition that the center column sum is exact to $O(h)$ was mistakenly defined as

$$\left| S_i - \frac{1}{h^2} \int_{x_i}^{x_{i+1}} (g(x) - y_{j-1}h) dx \right| \leq C_S h,$$

that is, $y_{j-1}h$ appears in the integrand, rather than just y_{j-1} . The correct definition appears here.

in the max norm:

$$|g(x) - \tilde{g}_{ij}(x)| \leq \left(\frac{50}{3}\kappa_{\max} + C_S\right)h^2 \quad \text{for all } x \in [x_i, x_{i+1}]. \quad (19)$$

See Section 4 of [24] for proofs of (18) and (19).

To summarize, once the 5×5 block of cells \tilde{B}_{ij} centered on the cell C_{ij} in which one wishes to reconstruct the interface has been rotated as described in Section 3, the interface reconstruction algorithm is based on choosing the slope m_{ij} of the piecewise linear approximation $\tilde{g}_{ij} = m_{ij}x + b_{ij}$ to the interface $g(x)$ to be one of the three divided differences of the column sums S_{i-1} , S_i and S_{i+1} from the 3×3 subblock B_{ij} centered on the cell C_{ij} as shown in (16). The best choice is when both column sums are exact, which — provided that the condition in (5) is satisfied — *is true in all but one case*.

This one case is the one in which the interface g satisfies (5) yet exits the i -th column S_i across its top edge as shown in Figure 4. (In this particular case the interface is *always monotonically increasing*.) Example 2 of [25] demonstrates that this case can occur for any value of h , no matter how small. However, in [25] it is proven that when this case occurs, one of the two divided differences of column sums, m_{ij}^l or m_{ij}^r , will still satisfy (18). Thus, choosing this quantity for the slope m_{ij} in $\tilde{g}_{ij} = m_{ij}x + b_{ij}$ still yields a pointwise second-order accurate approximation to g ; that is, the bound in (19) remains true. The following section contains a description of an algorithm for determining which of these cases is present, and hence which of the slopes in (16) — the first or the third — will yield a second-order accurate approximation to the interface in C_{ij} .

5. A description of the algorithm

Before proceeding one should note that there are a variety of ways to implement this algorithm. In particular, one can implement it so that it is not necessary rotate the 5×5 block \tilde{B}_{ij} . The description given here was chosen because it seems to be the easiest one to follow. Furthermore this is the way in which the algorithm was implemented in order to produce the computational results shown in Section 6.

There are two steps involved in computing the approximation $\tilde{g}_{ij}(x)$ to the interface $g(x)$ in a given cell C_{ij} .

- I. Determine the slope m_{ij} of the piecewise linear approximation

$$\tilde{g}_{ij}(x) = m_{ij}x + b_{ij}$$

to the interface $g(x)$ in the cell C_{ij} .

- II. Determine the y-intercept b_{ij} of $\tilde{g}_{ij}(x)$.

Step I. Given that the 5×5 block \tilde{B}_{ij} has been placed in the configuration described in Section 3 above, one need only consider the five cases listed below; namely Cases 1(a), 1(b) and Cases 2–4. From the discussion on column sums in Section 4 it is apparent that one needs two column sums that are either exact, or a left (resp., right) column sum that is exact and a center column sum that is exact to $O(h)$ as shown, for example, in Figure 4 (page 210).

The constraint in (5) on the interface $z(s)$ ensures that, once the 5×5 block of cells \tilde{B}_{ij} has been rotated as described above, only the following cases can occur:

- (1) The center column sum S_i is *exact to $O(h)$* , and hence satisfies (17), as shown, for example, in Figure 4, and one of the following two cases hold:
 - (a) The left column sum S_{i-1} is exact, in which case one uses the left-sided divided difference:

$$m_{ij} = m_{ij}^l = S_i - S_{i-1}. \quad (20)$$

- (b) The right column sum S_{i+1} is exact, in which case one uses the right-sided divided difference:

$$m_{ij} = m_{ij}^r = S_{i+1} - S_i. \quad (21)$$

- (2) All three column sums S_{i-1} , S_i and S_{i+1} are exact as shown, for example, in Figure 1. In this case one uses the centered difference of the left and right column sums:

$$m_{ij} = m_{ij}^c = \frac{1}{2}(S_{i+1} - S_{i-1}). \quad (22)$$

- (3) The left column sum S_{i-1} and center column sum S_i are exact. In this case one uses the left-sided divided difference:

$$m_{ij} = m_{ij}^l = S_i - S_{i-1}. \quad (23)$$

- (4) The center column S_i and right column sum S_{i+1} are exact. In this case one uses the right-sided divided difference:

$$m_{ij} = m_{ij}^r = S_{i+1} - S_i. \quad (24)$$

The various theorems and lemmas in [24; 25] prove that in each of the above cases the formulas in (20)–(24) result in a first-order accurate approximation m_{ij} to the first derivative $g'(x_c)$ of the interface at the point $x_c = \frac{1}{2}(x_i + x_{i+1})$, as shown in Equation (18).

Next is a description of the algorithm that one uses to obtain the correct slope given only the volume fraction information in the 3×5 block of cells \hat{B}_{ij} .

The algorithm to choose the slopes. Once the 5×5 block \tilde{B}_{ij} has been rotated as described in Section 3, one only uses the 3×5 portion \hat{B}_{ij} of \tilde{B}_{ij} to make the decision as to which of the cases listed above one uses for that particular cell C_{ij} . The algorithm for selecting the slope is as follows.

Case 1: (The center column sum S_i is not exact, but is exact to $O(h)$.) First one checks the cell C_{ij+2} . If $\Lambda_{ij+2} > 0$, then the cell *above* the center column contains some material 1 and hence the center column sum S_i is not exact. However, by Theorem 4 of [25] the condition on h in (5) ensures that S_i is exact to $O(h)$. Therefore, one next checks the left column sum S_{i-1} and right column sum S_{i+1} to determine which column sum is exact, and hence which difference one will use; that is, Case 1(a) or 1(b) from the list above. (The constraint in (5) will ensure that the column sums S_{i-1} and S_{i+1} are not both exact, but one of them will be.)

Case 1(a): If $\Lambda_{i-1,j+2} = 0$, the left column sum S_{i-1} is exact, and hence one uses the left-sided difference:

$$m_{ij} = m_{ij}^l = S_i - S_{i-1}.$$

Case 1(b): Otherwise, it must be the case that $\Lambda_{i+1,j+2} = 0$, and hence the right column sum is exact. Therefore, one uses the right-sided difference:

$$m_{ij} = m_{ij}^r = S_{i+1} - S_i.$$

Case 2: (The center column sum must be exact.) Otherwise, $\Lambda_{i,j+2} = 0$, and hence the center column sum S_i is exact. In this case one first checks to see which of the left and right column sums are exact. If both are exact, then one uses a centered difference. Otherwise one uses a one-sided difference with the center column and whichever of the left or right column sums is exact.

Case 2(a): If $\Lambda_{i-1,j+2} = 0$ and $\Lambda_{i+1,j+2} = 0$, then both the left column sum S_{i-1} and the right column sum S_{i+1} are exact. Therefore, one uses a centered difference, since it is one order more accurate than a one sided difference:

$$m_{ij} = m_{ij}^c = \frac{1}{2}(S_{i+1} - S_{i-1}).$$

Case 2(b): If only $\Lambda_{i-1,j+2} = 0$, and hence the right column sum S_{i+1} is not exact, then one uses the left-sided difference:

$$m_{ij} = m_{ij}^l = S_i - S_{i-1}.$$

Case 2(c): Otherwise, if only $\Lambda_{i+1,j+2} = 0$, and hence the left column sum S_{i-1} is not exact, then one uses the right-sided difference:

$$m_{ij} = m_{ij}^r = S_{i+1} - S_i.$$

Step II. Once the slope m_{ij} has been found the constraint

$$\tilde{\Lambda}_{ij}(\tilde{g}) = \Lambda_{ij}(g),$$

where $\tilde{\Lambda}_{ij}(\tilde{g})$ denotes the fraction of material 1 in the ij -th cell due to \tilde{g} , immediately determines b_{ij} . In other words, once the 5×5 block of cells \tilde{B}_{ij} has been appropriately rotated, b_{ij} is a single valued function of $\tilde{\Lambda}_{ij}(\tilde{g})$ and m_{ij} :

$$b_{ij} = b_{ij}(\tilde{\Lambda}_{ij}(\tilde{g}), m_{ij}).$$

There are a variety of formulas one can employ to determine b_{ij} given m_{ij} . For example, there is an approach that is based on representing the boundary of the portion of the cell C_{ij} that contains material 1 by directed line segments and using the divergence theorem to compute the volume fraction Λ_{ij} developed by S. G. Roberts and used in [26]. There is the approach developed by J. S. Saltzman and used in [23] that is based on employing a coordinate system in which the approximate interface $\tilde{g}_{ij}(x)$ is given by

$$n_{ij}^x x + n_{ij}^y y = \sigma,$$

where $\mathbf{n}_{ij} = (n_{ij}^x, n_{ij}^y)$ is the unit normal to $\tilde{g}_{ij}(x)$ that points away from the material 1 and σ is the distance from \tilde{g}_{ij} to (x_i, y_j) , the lower left hand corner of the cell C_{ij} . In work with Kothe et al. [8; 10; 32; 11], M. W. Williams developed algorithms for working on three-dimensional hexahedral and other unstructured meshes. Details of this work may also be found in Williams' Ph.D. thesis [33]. Finally, an article by Scardovelli and Zaleski [29] describes a collection of formulas one may use on two and three dimensional rectangular grids.

The algorithm that was used to compute the computational example shown in Section 6 of this article is based on determining which of the three polygons the approximate interface $\tilde{g}_{ij}(x)$ forms when it passes through the cell C_{ij} :

- (1) a triangle,
- (2) the complement of a triangle in a square, and
- (3) a trapezoid.

In other words, material 1 is contained in a region that has the shape of one of the three polygons listed above.

Given the volume fraction Λ_{ij} — and hence the volume⁹ V_{ij} of material 1 in the ij -th cell — and the slope m_{ij} , one can write down algebraic formulas for each of these polygons. In this way the polygon with the correct volume is readily identified, and with it the point of intersection of the approximate interface $\tilde{g}_{ij}(x)$ with two of

⁹As previously noted, strictly speaking one is given the *area* of material 1 in the ij -th cell. By convention this area is referred to as *the volume* of material 1 in the ij -th cell.

the four grid lines: $x = x_i$, $x = x_{i+1}$, $y = y_j$ and $y = y_{j+1}$ that form the edges of the cell C_{ij} . Given this information, the y -intercept b_{ij} is easily found.

Note that several of the other algorithms for representing the approximate interface listed above allow one to design the method so that it is not necessary to rotate the 5×5 block of cells \tilde{B}_{ij} . However, the implementation of such an algorithm may be more complex than the one described here.

6. A computational example

Table 1 contains the max norm error from a computation in which the interface reconstruction algorithm described in this paper is used to approximate $\cos x$ for $0 \leq x \leq \pi$ on square grids with cell sizes varying from 32^{-1} to 4096^{-1} . The error reported in the table is computed according to the formula

$$l^\infty \text{error} = \max_{C_{ij}} \left\{ \max_{x \in [x_i, x_{i+1}]} |g(x) - \tilde{g}_{ij}(x)| \right\}, \tag{25}$$

where $\max_{x \in [x_i, x_{i+1}]} |g(x) - \tilde{g}_{ij}(x)|$ is computed at 1000 points between the end-points x_l (resp., x_r) at which the curve $g(x)$ enters (resp., exits) the cell C_{ij} and the outer maximum in (25) is taken over all cells C_{ij} that satisfy $0 < \Delta_{ij} < 1$.

The third column contains the error (25) for the cell size reported in the second column. The fourth column contains the theoretical error bound from [25], which is quoted in Equation (2) (and also in Equation (26) below). Note that for all values of Δx the actual error is two orders of magnitude *less than* the theoretical error bound.

The last column of Table 1 contains the *convergence rate*. For a particular value of $\Delta x = 2^{-k}$, the convergence rate is defined to be the rate at which the error would have to decrease in going from $\Delta x = 2^{-(k-1)}$ to $\Delta x = 2^{-k}$ in order to achieve the

k	cell size $\Delta x = 2^{-k}$	l^∞ error	theoretical error bound	convergence rate
05	32^{-1}	$1.07 \cdot 10^{-4}$	$8.43 \cdot 10^{-2}$	2.19
06	64^{-1}	$2.67 \cdot 10^{-5}$	$2.11 \cdot 10^{-2}$	2.00
07	128^{-1}	$7.26 \cdot 10^{-6}$	$5.27 \cdot 10^{-3}$	1.88
08	256^{-1}	$1.80 \cdot 10^{-6}$	$1.32 \cdot 10^{-3}$	2.02
09	512^{-1}	$4.45 \cdot 10^{-7}$	$3.29 \cdot 10^{-4}$	2.01
10	1024^{-1}	$1.12 \cdot 10^{-7}$	$5.95 \cdot 10^{-5}$	1.99
11	2048^{-1}	$2.83 \cdot 10^{-8}$	$2.06 \cdot 10^{-5}$	1.99
12	4096^{-1}	$7.13 \cdot 10^{-9}$	$5.14 \cdot 10^{-6}$	1.99

Table 1. The max norm of the error from the computation of $\cos x$ for $0 \leq x \leq \pi$.

error that is shown for $\Delta x = 2^{-k}$. In other words,

$$\text{convergence rate in the row with } \Delta x = 2^{-k} := \log_2 \left(\frac{\text{error}(2^{-(k-1)})}{\text{error}(2^{-k})} \right),$$

where $\text{error}(2^{-k})$ denotes the error in the max norm when $\Delta x = 2^{-k}$. It is apparent that the error in the max norm decreases at a rate commensurate with a method that is second-order accurate in the max norm as claimed.

7. Conclusions

The main result of [24; 25] is a proof that

$$|g(x) - \tilde{g}_{ij}(x)| \leq \left(\frac{50}{3} \kappa_{\max} + C_S \right) h^2 \quad \text{for all } x \in [x_i, x_{i+1}], \quad (26)$$

where $\tilde{g}_{ij}(x)$ is the volume-of-fluid approximation to the interface $g(x)$ in the cell C_{ij} that is described in this paper, κ_{\max} is the maximum curvature of the interface as defined in (4), x_i and x_{i+1} denote the left and right edges respectively of the cell C_{ij} , h is the length of each side of the square grid cell C_{ij} and

$$C_S = \frac{\sqrt{3}}{2} \left\{ (2\sqrt{2} - 1) 4\sqrt{\kappa_{\max}} + \left(1 - \frac{7(1 + \sqrt{2})}{20} \right) \frac{32}{3} (\sqrt{\kappa_{\max}})^3 \right\}^2.$$

The bound in (26) holds whenever the grid size h and the maximum value

$$\kappa_{\max} = \max_s |\kappa(s)|$$

of the curvature $\kappa(s)$ of the interface $z(s)$ in the 3×3 block of cells B_{ij} satisfies

$$h \leq \frac{C_h}{\kappa_{\max}}, \quad \text{where } C_h = \frac{1}{25}. \quad (27)$$

However, in [24; 25] there are no examples of algorithms for finding the volume-of-fluid approximation $\tilde{g}_{ij}(x)$ in each cell C_{ij} which contains a portion of the interface. This article contains a description of one such algorithm. This algorithm is new and has not appeared previously in the scientific literature. As shown in Table 1 the computations to approximate $\cos x$ on the interval $[0, \pi]$ shown in Section 6 are consistent with the theoretical error bounds in [24; 25]. In other words, the computational approximation of $\cos x$ made with this new algorithm is consistent with the claim that it is second order accurate in the max norm provided that the interface $g \in C^2$ and (27) is satisfied.

It may be possible for the interface to pass through the center cell, then exit the 3×3 block B_{ij} , wander around the computational domain, and reenter the 3×3 block B_{ij} and the center cell C_{ij} again. For the purposes of this paper it is assumed that this does not happen. When implementing the algorithm described in this paper, one can design the code to automatically check for such cases and flag the 3×3

block B_{ij} for grid refinement, so that no cell contains two instances of the interface in a configuration such as the one just described.

In [21] J. E. Pilliod and Puckett described two volume-of-fluid interface reconstruction algorithms they had developed, and which they named the *Least Squares Volume-of-Fluid Interface Reconstruction Algorithm* (LVIRA) and the *Efficient Least Squares Volume-of-Fluid Interface Reconstruction Algorithm* (ELVIRA). They then presented computations with these algorithms on both C^2 and C^0 interfaces. When the underlying exact solution was a circle, the LVIRA and ELVIRA algorithms were shown to be second-order accurate in the max norm.

In all of the other computations they computed the errors in the *averaged l^1* norm; that is, the l^1 norm averaged over 1000 random perturbations of the problem. For example, the l^1 error reported in approximating a circle was an average of the errors obtained when approximating 1000 different unit circles in which the center of the circle was chosen at random. They then compared the errors with errors obtained when they used several other widely used volume-of-fluid interface reconstruction algorithms such as SLIC [19] and the method developed by Parker and Youngs [20]. The only other algorithm that was close to being second-order accurate in the averaged l^1 norm consisted of taking the centered difference for the slope — that is, $m_{ij} = m_{ij}^c$, where m_{ij}^c is defined in (16).

It is not clear whether the proofs in [24; 25] apply to the LVIRA and ELVIRA algorithms. Hence, it is not clear whether LVIRA and ELVIRA are second-order accurate in the max norm, or in the l^1 and l^2 norms when the errors are not averaged over many computations. Future work should include a study of this issue and a direct comparison between the algorithm presented here and the LVIRA and ELVIRA algorithms.

One should also note that both the LVIRA and ELVIRA algorithms, as well as the algorithm presented here, reconstruct lines *exactly*. It is an open problem to prove whether or not this is a sufficient condition for the algorithm to be second-order accurate when the underlying interface is C^2 .

Corollary 22 in [24] states that the algorithm presented in this paper with slope $m_{ij} = 0$ (i.e., the piecewise constant or “stair-step” volume-of-fluid interface reconstruction algorithm) will be first-order accurate whenever the interface is C^1 rather than C^2 . (See footnote 10 in [24] regarding how smooth the interface must be in order to prove Corollary 22.) Future work should include an exploration of how well the algorithm presented here approximates interfaces that are less than C^2 .

Finally, when the interface reconstruction algorithm is coupled to an adaptive mesh refinement algorithm, the parameter

$$H_{\max} = C_h(\kappa_{\max})^{-1},$$

where κ_{\max} is the maximum curvature of the interface over the 3×3 block of cells

B_{ij} centered on a given cell C_{ij} , can be used to develop a criterion for determining when to increase the resolution of the grid. Namely, the computation of the interface in C_{ij} is *under-resolved* whenever

$$h > H_{\max},$$

and hence the grid needs to be refined in a neighborhood of the block B_{ij} .

References

- [1] I. Aleinov and E. G. Puckett, *Computing surface tension with high-order kernels*, Proceedings of the 6th International Symposium on Computational Fluid Dynamics (Lake Tahoe, CA) (K. Oshima, ed.), 1995, pp. 6–13.
- [2] J. U. Brackbill, D. B. Kothe, and C. Zemach, *A continuum method for modeling surface tension*, J. Comput. Phys. **100** (1992), no. 2, 335–354. [MR 93c:76008](#) [Zbl 0775.76110](#)
- [3] A. J. Chorin, *Flame advection and propagation algorithms*, J. Comput. Phys. **35** (1980), no. 1, 1–11. [MR 81d:76061](#) [Zbl 0425.76086](#)
- [4] ———, *Curvature and solidification*, J. Comput. Phys. **57** (1985), no. 3, 472–490. [MR 86d:80001](#) [Zbl 0555.65085](#)
- [5] L. F. Henderson, P. Colella, and E. G. Puckett, *On the refraction of shock waves at a slow-fast gas interface*, J. Fluid Mech. **224** (1991), 1–27.
- [6] C. W. Hirt and B. D. Nichols, *Volume of fluid (VOF) method for the dynamics of free boundaries*, J. Comput. Phys. **39** (1981), 201–225.
- [7] R. M. Hurst, *Numerical approximations to the curvature and normal of a smooth interface using high-order kernels*, MS Thesis, Department of Mathematics, University of California, Davis, December 1995, Shields Library Special Collections LD781.D5j 1995 H873.
- [8] D. R. Korzekwa, D. B. Kothe, K. L. Lam, E. G. Puckett, P. K. Tubesing, and M. W. Williams, *A second-order accurate, linearity-preserving volume tracking algorithm for free surface flows on 3-d unstructured meshes*, Proceedings of the 3rd ASME /JSME Joint Fluids Engineering Conference (San Francisco, CA), FEDSM99-7109, American Society of Mechanical Engineers, 1999.
- [9] D. B. Kothe, J. R. Baumgardner, S. T. Bennion, J. H. Cerutti, B. J. Daly, K. S. Holian, E. M. Kober, S. J. Mosso, J. W. Painter, R. D. Smith, and M. D. Torrey, *PAGOSA: A massively-parallel, multi-material hydro-dynamics model for three-dimensional high-speed flow and high-rate deformation*, Technical Report LA-UR-92-4306, Los Alamos National Laboratory, 1992.
- [10] D. B. Kothe, E. G. Puckett, and M. W. Williams, *Approximating interface topologies with applications to interface tracking algorithms*, Proceedings of the 37th AIAA Aerospace Sciences Meetings (Reno, NV), American Institute of Aeronautics and Astronautics, 1999, pp. 1–9.
- [11] ———, *Robust finite volume modeling of 3-d free surface flows on unstructured meshes*, Proceedings of the 14th AIAA Computational Fluid Dynamics Conference (Norfolk, VA), American Institute of Aeronautics and Astronautics, 1999, pp. 1–6.
- [12] P. Lax and B. Wendroff, *Systems of conservation laws*, Comm. Pure Appl. Math. **13** (1960), 217–237. [MR 22 #11523](#) [Zbl 0152.44802](#)
- [13] R. J. LeVeque, *Numerical methods for conservation laws*, Lectures in Math. ETH Zürich, Birkhäuser, Basel, 1990. [MR 91j:65142](#) [Zbl 0723.65067](#)

- [14] G. H. Miller and P. Colella, *A conservative three-dimensional Eulerian method for coupled solid-fluid shock capturing*, J. Comput. Phys. **183** (2002), no. 1, 26–82. [MR 2003j:76080](#) [Zbl 1057.76558](#)
- [15] G. H. Miller and E. G. Puckett, *Edge effects in molybdenum-encapsulated molten silicate shock wave targets*, J. Appl. Phys. **75** (1994), no. 3, 1426–1434.
- [16] ———, *A high-order Godunov method for multiple condensed phases*, J. Comput. Phys. **128** (1996), no. 1, 134–164.
- [17] B. D. Nichols, C. W. Hirt, and R. S. Hotchkiss, *SOLA-VOF: A solution algorithm for transient fluid flow with multiple free boundaries*, Technical Report LA-8355, Los Alamos National Laboratory, August 1980.
- [18] W. F. Noh and P. R. Woodward, *SLIC (Simple Line Interface Calculation)*, Technical Report UCRL-77651, Lawrence Livermore National Laboratory, August 23 1976.
- [19] ———, *SLIC (Simple Line Interface Calculation)*, Lecture Notes in Physics (A. I. van der Vooren and P. J. Zandbergen, eds.), vol. 59, Springer, New York, 1976, pp. 330–340.
- [20] B. J. Parker and D. L. Youngs, *Two and three dimensional Eulerian simulation of fluid flow with material interfaces*, Technical Report 01/92, UK Atomic Weapons Establishment, Aldermaston, Berkshire, Feb 1992.
- [21] J. E. Pilliod, Jr. and E. G. Puckett, *Second-order accurate volume-of-fluid algorithms for tracking material interfaces*, J. Comput. Phys. **199** (2004), no. 2, 465–502. [MR 2005d:65145](#) [Zbl 1126.76347](#)
- [22] S. Popinet and S. Zaleski, *A front-tracking algorithm for accurate representation of surface tension*, Int. J. for Numer. Methods in Fluids **30** (1999), no. 6, 775–793. [Zbl 0940.76047](#)
- [23] E. G. Puckett and J. S. Saltzman, *A 3D adaptive mesh refinement algorithm for multimaterial gas dynamics*, Phys. D **60** (1992), no. 1-4, 84–93. [MR 93i:76062](#) [Zbl 0779.76059](#)
- [24] E. G. Puckett, *On the second-order accuracy of volume-of-fluid interface reconstruction algorithms: Convergence in the max norm*, Commun. Appl. Math. Comput. Sci. **5** (2010), 99–148. [MR 2600824](#) [Zbl 05709095](#)
- [25] E. G. Puckett, *On the second-order accuracy of volume-of-fluid interface reconstruction algorithms II: An improved constraint on the cell size*, CAMCoS (2010), Submitted for publication.
- [26] E. G. Puckett and S. G. Roberts, *A volume-of-fluid method for modeling flow by mean curvature*, 1990, work performed at the Australian National University.
- [27] W. J. Rider and D. B. Kothe, *Reconstructing volume tracking*, J. Comput. Phys. **141** (1998), no. 2, 112–152. [MR 99a:65200](#) [Zbl 0933.76069](#)
- [28] R. Scardovelli and S. Zaleski, *Direct numerical simulation of free-surface and interfacial flow*, Annual review of fluid mechanics (C. Cambon and J. F. Scott, eds.), vol. 31, Annual Reviews, Palo Alto, CA, 1999, pp. 567–603. [MR 99m:76002](#)
- [29] R. Scardovelli and S. Zaleski, *Analytical relations connecting linear interfaces and volume fractions in rectangular grids*, J. Comput. Phys. **164** (2000), no. 1, 228–237. [MR 1786246](#) [Zbl 0993.76067](#)
- [30] M. D. Torrey, L. D. Cloutman, R. C. Mjolsness, and C. W. Hirt, *NASA-VOF2D: A computer program for incompressible flows with free surfaces*, Technical Report LA-10612-MS, Los Alamos National Laboratory, December 1985.
- [31] M. D. Torrey, R. C. Mjolsness, and L. R. Stein, *NASA-VOF3D: A three-dimensional computer program for incompressible flows with free surfaces*, Technical Report LA-11009-MS, Los Alamos National Laboratory, July 1987.

- [32] M. W. Williams, D. B. Kothe, and E. G. Puckett, *Accuracy and convergence of continuum surface-tension models*, Fluid dynamics at interfaces (W. Shyy, ed.), Cambridge Univ. Press, 1999, pp. 294–305. [MR 1719592](#) [Zbl 0979.76014](#)
- [33] M. W. Williams, *Numerical methods for tracking interfaces with surface tension in 3-d mold-filling processes*, Ph.D. thesis, University of California, Davis, 2000.

Received February 23, 2010.

ELBRIDGE GERRY PUCKETT: egpuckett@ucdavis.edu

University of California, Davis, Department of Mathematics, One Shields Avenue, Davis, CA 95616, United States

<http://www.math.ucdavis.edu/>

Communications in Applied Mathematics and Computational Science

pjm.math.berkeley.edu/camcos

EDITORS

MANAGING EDITOR

John B. Bell

Lawrence Berkeley National Laboratory, USA

jbbell@lbl.gov

BOARD OF EDITORS

Marsha Berger	New York University berger@cs.nyu.edu	Ahmed Ghoniem	Massachusetts Inst. of Technology, USA ghoniem@mit.edu
Alexandre Chorin	University of California, Berkeley, USA chorin@math.berkeley.edu	Raz Kupferman	The Hebrew University, Israel raz@math.huji.ac.il
Phil Colella	Lawrence Berkeley Nat. Lab., USA pcollella@lbl.gov	Randall J. LeVeque	University of Washington, USA rjl@amath.washington.edu
Peter Constantin	University of Chicago, USA const@cs.uchicago.edu	Mitchell Luskin	University of Minnesota, USA luskin@umn.edu
Maksymilian Dryja	Warsaw University, Poland maksymilian.dryja@acn.waw.pl	Yvon Maday	Université Pierre et Marie Curie, France maday@ann.jussieu.fr
M. Gregory Forest	University of North Carolina, USA forest@amath.unc.edu	James Sethian	University of California, Berkeley, USA sethian@math.berkeley.edu
Leslie Greengard	New York University, USA greengard@cims.nyu.edu	Juan Luis Vázquez	Universidad Autónoma de Madrid, Spain juanluis.vazquez@uam.es
Rupert Klein	Freie Universität Berlin, Germany rupert.klein@pik-potsdam.de	Alfio Quarteroni	Ecole Polytech. Féd. Lausanne, Switzerland alfio.quarteroni@epfl.ch
Nigel Goldenfeld	University of Illinois, USA nigel@uiuc.edu	Eitan Tadmor	University of Maryland, USA etadmor@cscamm.umd.edu
	Denis Talay	INRIA, France denis.talay@inria.fr	

PRODUCTION

apde@mathscipub.org

Silvio Levy, Scientific Editor

Sheila Newbery, Senior Production Editor

See inside back cover or pjm.math.berkeley.edu/camcos for submission instructions.

The subscription price for 2010 is US \$70/year for the electronic version, and \$100/year for print and electronic. Subscriptions, requests for back issues from the last three years and changes of subscribers address should be sent to Mathematical Sciences Publishers, Department of Mathematics, University of California, Berkeley, CA 94720-3840, USA.

Communications in Applied Mathematics and Computational Science, at Mathematical Sciences Publishers, Department of Mathematics, University of California, Berkeley, CA 94720-3840 is published continuously online. Periodical rate postage paid at Berkeley, CA 94704, and additional mailing offices.

CAMCoS peer review and production are managed by EditFLOW™ from Mathematical Sciences Publishers.

PUBLISHED BY
 **mathematical sciences publishers**
<http://www.mathscipub.org>

A NON-PROFIT CORPORATION

Typeset in L^AT_EX

Copyright ©2010 by Mathematical Sciences Publishers

Communications in Applied Mathematics and Computational Science

vol. 5

no. 2

2010

- On the accuracy of finite-volume schemes for fluctuating hydrodynamics 149
ALEKSANDAR DONEV, ERIC VANDEN-EIJNDEN, ALEJANDRO
GARCIA and JOHN BELL
- A volume-of-fluid interface reconstruction algorithm that is second-order
accurate in the max norm 199
ELBRIDGE GERRY PUCKETT
- Implicit particle filters for data assimilation 221
ALEXANDRE CHORIN, MATTHIAS MORZFELD and XUEMIN TU
- Parallel in time algorithms with reduction methods for solving chemical
kinetics 241
ADEL BLOUZA, LAURENT BOUDIN and SIDI MAHMOUD KABER
- A hybrid parareal spectral deferred corrections method 265
MICHAEL L. MINION